Assessing the Huang-Brown description of tie chains for charge transport in conjugated polymers

Kaichen Gu[†], Chad R. Snyder[‖], Jonathan Onorato[‡], Christine K. Luscombe[‡,#,¶], August W. Bosse[§], Yueh-Lin Loo[†,⊥,*]

[†] Department of Chemical and Biological Engineering, Princeton University, Princeton, New Jersey 08544, United States

[‖] Materials Science and Engineering Division, National Institute of Standards and Technology, Gaithersburg, Maryland 20899, United States

[‡] Materials Science and Engineering Department, University of Washington, Seattle, Washington 98195-2120, United States

[§] Corporate Strategic Research, ExxonMobil Research and Engineering Company, Annandale, New Jersey 08801, United States

[⊥] Andlinger Center for Energy and the Environment, Princeton University, Princeton, NJ 08544New Jersey 08544, United States

[#] Department of Chemistry, University of Washington, Seattle, Washington 98195-1700, United States

[¶] Molecular Engineering and Sciences Institute, University of Washington, Seattle, Washington 98195-1652, United States

ABSTRACT: Intercrystallite molecular connections are widely recognized to tremendously impact the macroscopic properties of semicrystalline polymers. Because it is challenging to directly probe such connections, theoretical frameworks have been developed to quantify their concentrations and predict the mechanical properties that result from these connections. Tie-chain connectivity similarly impacts the electrical properties in semicrystalline conjugated polymers. Yet, its quantitative impact has eluded the community. Here, we assess the Huang-Brown model, a framework commonly used to describe the structural origins of mechanical properties in polyolefins, to quantitatively elucidate the effect of tie chains on the electrical properties of a model conjugated polymer. We found that a critical tie-chain fraction of 10^{-3} is needed to support macroscopic charge transport, below which intercrystallite connectivity limits charge transport, and above which intracrystallite disorder is the bottleneck. Extending the Huang-Brown framework to conjugated polymers enables the prediction of macroscopic electrical properties based on experimentally-accessible morphological parameters. Our study implicates the importance of long and rigid polymer chains for efficient charge transport over device length scales.

The presence of intercrystallite molecular connections dictates the mechanical properties of semicrystalline polymers.[1–3] There has thus been a strong push to develop predictive frameworks based on experimentally accessible and tunable variables to quantify the concentrations of such connections, and accordingly to understand their impact on macroscopic properties.[4,5] Of these endeavors, the statistical approach developed by Huang and Brown[6,7] has gained substantial traction for capturing the microstructural origins of mechanical properties of polyolefin resins, especially their resistance to slow crack growth.[8] Inspired by the success with which the polyolefin industry has been able to use the Huang-Brown model to predictively produce resins with pre-specified mechanical properties, we assessed this framework to quantitatively describe charge transport in a model semicrystalline conjugated polymer. While the organic electronics community has generally acknowledged the role tie chains play in facilitating macroscopic charge transport,[9] and there exists an abundance of indirect evidence that speaks to their importance in the form of molar-mass-dependent field-effect mobility in the literature,[10–14] our assessment and application of the Huang-Brown model provides the first quantification of the impact of tie chains on macroscopic electrical properties in semicrystalline conjugated polymer systems.

We started with batches of model poly(3-hexylthiophene), or P3HT, with distinct molar mass (M) and low dispersity ($Đ$), synthesized per literature.[15,16] We systematically blended different batches in varying mass ratios to produce unique molar mass distributions as a way to access samples having different tie-chain fractions.[14] We obtained the absolute molar mass distribution of these P3HT samples by a combination of size exclusion chromatography (SEC) and nuclear magnetic resonance (NMR) spectroscopy end-group analysis; we measured the crystallinity and crystalline domain thickness of the same samples by differential scanning calorimetry (DSC). Optical, electrical, and calorimetric measurements were all performed on drop-cast P3HT samples that have undergone the same processing history to allow for meaningful comparison. Using these experimentally-obtained physical properties as input parameters, we extended the Huang-Brown model to calculate the tie-chain fraction in P3HT thin films. We find the Huang-Brown model to effectively describe tie-chain contributions to charge transport; percolation sets in when the tie-chain fraction is $\approx 10^{-3}$, below which charge transport is limited by intercrystallite connectivity, and above which charge

transport is limited by intracrystallite structural disorder. Despite its simplicity, the Huang-Brown model offers a first-order guide on the polymer-chain characteristics and molar mass distributions to maximize charge transport.

Figure 1 shows field-effect mobilities of thin-film transistors comprising P3HT blends as active layers. Here, a notation of P3HT_x is used to denote P3HT having a number-average molar mass (M_n) of x kg mol^{-1}; a notation of P3HT_x/y is used to denote P3HT homopolymer blends comprising a lower-M P3HT of M_n = x kg mol^{-1} and a higher-M P3HT of M_n = y kg mol^{-1}. For transistors comprising P3HT_5/20 (**Figure 1a**) and P3HT_5/40 (**Figure 1b**), the mobility initially increases with increasing loadings of the higher-M P3HT. This trend is consistent with the notion that increasing the fraction of the higher-M polymer increases the probability of forming tie chains, which has in turn been correlated with improved macroscopic charge transport.[13,17–19] The field-effect mobility then levels off, presumably when there is sufficient connectivity between crystalline domains. Despite the qualitatively similar trends, subtle differences exist between P3HT_5/20 and P3HT_5/40. We particularly note the difference in the threshold molar mass at which the mobility plateaus, at mass-average molar masses of ≈10 kg mol^{-1} and ≈35 kg mol^{-1} for transistors comprising P3HT_5/20 and P3HT_5/40, respectively. We surmise this quantitative difference stems from differences in domain connectivity in the transistors comprising these two blends. As a control experiment, we measured the mobilities of transistors comprising blends of the two highest-M batches of P3HT. These mobilities remain invariant across the composition window (P3HT_20/40 in **Figure 1c**), suggesting that P3HT_20, by itself and in the absence of P3HT_40, has sufficient tie chains to bridge neighboring crystalline domains to support macroscopic charge transport.

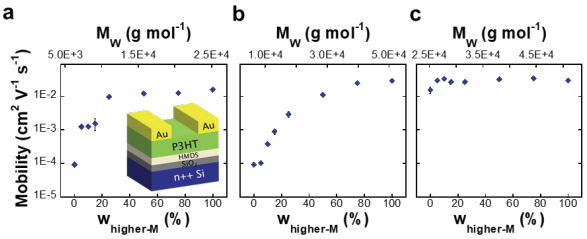

Figure 1. Field-effect mobility of transistors comprising (a) P3HT_5/20, (b) P3HT_5/40, and (c) P3HT_20/40, as a function of the mass fraction of the higher-M P3HT in each blend. The inset in (a) illustrates the bottom-gate, top-contact configuration of transistors used in this study. Error bars here and elsewhere correspond to the best estimate of one standard error in the experimental uncertainty.

In order to gain further insight into the role of domain connectivity on charge transport, we quantified the probability of tie-chain formation with the Huang-Brown model.[6,7] The Huang-Brown model assumes Fischer's solidification scheme,[20] in which the characteristic size of polymer chains in the melt is preserved on rapid crystallization. P3HT is known to crystallize rapidly;[21,22] we thus assumed that its solidification is consistent with Fischer's solidification scheme. The Huang-Brown model is centered on the assumption that polymer chains with end-to-end distances greater than, or equal to, the distance between adjacent crystallites will form tie chains. For a polymer chain of a given molar mass (M), Huang and Brown argued that the probability of forming a tie chain spanning two neighboring crystalline domains that are a critical distance, d_c, apart is described by Equation (1) below:

$$P(M) = \frac{\int_{d_c}^{\infty} r^2 \exp\left(-\frac{3r^2}{2Nl_K^2}\right) dr}{\int_{0}^{\infty} r^2 \exp\left(-\frac{3r^2}{2Nl_K^2}\right) dr} \quad (1)$$

This probability distribution assumes Gaussian chain statistics where N is the number of effective Kuhn segments and l_K is the Kuhn length ($l_K = 2*L_p$ where L_p is the persistence length of P3HT, 2.9 nm)[23]. In the molar mass range we access, the contour length of P3HT is significantly greater than its persistence length; Gaussian chain statistical behavior is thus valid.[24] We estimate the contour length of P3HT chains to be comparable to its persistence length at a critical molar mass of ≈1200 g mol^{-1}.

In order to determine the critical distance over which tie chains span, we need to first estimate the crystalline domain thickness and the characteristic distance between crystalline domains. We extracted these parameters from the onset melting temperature (T_m) and the enthalpy of fusion (ΔH_f) measured by DSC. Specifically, the crystalline domain thickness along the chain-axis direction was estimated from T_m using the following relationship:[25,26]

$$l_c = c \times \frac{bT_m - aT_m^0}{T_m^0 - T_m} \quad (2)$$

where a and b are constants with a = -5.4 ± 0.5 and b = -1.6 ± 0.4; T_m^0 is the equilibrium melting temperature of P3HT (545 ± 6 K),[26] and c is the repeat distance of the thiophene mer (0.39 nm).[27]

Crist and Mirabella demonstrated that a correction factor of (T_m^0/T_m) accounts for crystal-size effects on apparent crystallinity as characterized through the enthalpy of fusion.[28] Hence, we calculated the crystallite-size corrected crystallinity by:[26]

$$\chi_c = \frac{\Delta H_f}{\Delta H_u} \frac{T_m^0}{T_m} \quad (3)$$

where ΔH_u is the enthalpy of fusion of a perfect P3HT crystal (49 J g^{-1}).[26] We estimated the characteristic distance between crystalline domains by:[8]

$$l_a = l_c \times \frac{\rho_c(1-\chi_c)}{\rho_a \chi_c} \quad (4)$$

where ρ_c is the crystalline density (1.13 g cm^{-3}) and ρ_a is the amorphous density (1.094 g cm^{-3}) of P3HT.[29] Here, we calculated $P(M)$ using (l_c+l_a) as the critical distance for which tie chains form in these P3HT blends.

Strictly speaking, equation (1) is only applicable for monodisperse systems. For any practical P3HT having a finite distribution of molar mass, $f(M)$, where $f(M)dM$ is the mole fraction of polymer with molar masses between M and M + dM, the probability calculated from equation (1) is essentially a weighting factor for each slice of the molar mass distribution. The overall probability of tie-chain formation can thus be calculated by integrating the probability of forming a tie chain over the entire molar mass distribution.[30]

In order to more precisely capture the electrical connectivity across the crystallites in the charge transport direction, especially in anisotropic systems, it is likely that the integral in (1) will need to be modified. For example, one might consider the characteristic size of the chains in a

specific direction of interest (e.g., the charge transport direction). Following Huang and Brown, the fraction of tie chains along the charge-transport direction can be approximated by multiplying the overall probability by a pre-factor of 1/3.

$$f_{TC} \cong \frac{1}{3}\int_0^\infty f(M)P(M)dM \qquad (5)$$

We note, however, while the exact value of the pre-factor may depend on the film morphology, it does not alter the relative tie-chain fractions across the different blends that adopt the same nominal structure.

Figure 2a shows the field-effect mobility of transistors comprising all the blends examined in this study as a function of f_{TC}. We find charge transport to be highly dependent on the presence of tie chains. With the initial rise in tie-chain fraction, we observe a drastic improvement in field-effect mobility, presumably because more tie chains provide additional conductive pathways linking neighboring crystalline domains in the sub-percolation regime. Interestingly, the mobility data extracted from transistors comprising blends of P3HT_5/20 and 5/40 collapse onto a single universal curve when plotted as a function of tie-chain fraction, suggesting it, as opposed to the molar mass of the conjugated polymer, to be the appropriate scaling variable that governs charge transport. Our analysis estimates, for the first time, that only 10^{-3} of all chains need to form tie chains in order for P3HT to develop a percolated network to support macroscopic charge transport. Once the tie-chain fraction is above this percolation threshold, the field-effect mobility becomes independent of tie-chain fraction and levels off at ≈0.02 $cm^2 V^{-1} s^{-1}$.

We attribute the effectiveness of the Huang-Brown model in describing charge transport in P3HT to an alignment between the quasi-static electrical measurements with which we extracted field-effect mobility and the fundamental assumptions of the framework. In transistor measurements, the chain conformation is largely unperturbed, consistent with the framework's foundational assumption. The model further assumes that all intercrystallite molecular connections take the form of tie chains; chain entanglements are not considered in this framework.[6,31,32] Consistent with this assumption, entanglements contribute negligibly to electrical connectivity compared to tie chains because charge carriers still have to hop between entangled chains to access neighboring crystalline domains, as schematically shown in **Figure 2b**.

We argue that this alignment between the model's assumptions and electrical measurements is stronger than that with mechanical measurements. In contrast to quasi-static electrical measurements, mechanical testing to extract tensile strength, toughness, strain-hardening modulus and other properties involves significant deformation of the samples so the foundational assumption that polymer chains retain their characteristic size is almost certainly invalid. Adding to this deviation from the model's assumption is the fact that chain entanglements, which are capable of transferring stress between neighboring crystallites, contribute substantively to mechanical strength. Neglecting chain entanglements thus limits the accurate capture of the structural origins of mechanical strength in semicrystalline polymers. The assumptions underlying the Huang-Brown model hence result in intrinsic limitations in developing relationships between structure and mechanical properties, but these limitations are seemingly circumvented in elucidating how structure impacts the electrical properties of conjugated polymers.

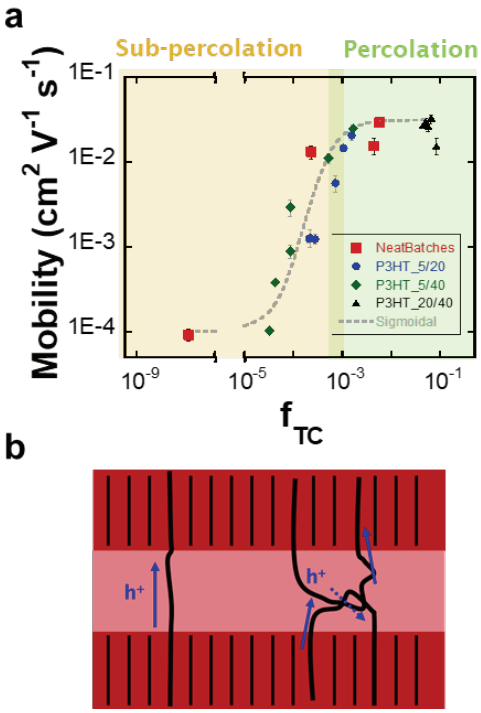

Figure 2. (a) Field-effect mobility of transistors comprising P3HT blends as a function of the tie-chain fraction (f_{TC}). The f_{TC} calculations were performed using the long period (l_c + l_a) as the critical distance required for tie chain formation. A sigmoidal line has been added for visual guide. (b) Schemes of the two types of intercrystallite molecular connections, namely tie chains (left) and chain entanglements (right). To arrive at the adjacent crystallite, charge carriers travel directly across tie chains but have to hop between chains across the entanglements.

In applying this statistical approach, we needed to define the critical distance beyond which a tie chain can be established, corresponding to the minimum distance that polymer chains need to span in order to electrically bridge two neighboring crystalline domains. While the above detailed our analysis based on a critical distance of (l_c + l_a), we assessed how sensitive the tie-chain fraction in P3HT_5/40 is when different critical distances are used. Outlined in Supporting Information and summarized in **Figure S1,** we see that the absolute value of the calculated tie-chain fraction strongly depends on the choice of critical distance, with larger critical distances resulting in smaller f_{TC}. However, the relative f_{TC} across the different P3HT blends is insensitive to the choice of critical distance, implying the robustness of the model.[7]

With the Huang-Brown model, we can effectively explain the rise in mobility with increasing loadings of the higher-M P3HT, and attribute the onset of percolation to a critical tie-chain fraction at ≈10^{-3}. We further sought to explain why the mobility plateaus beyond this percolation threshold. The channel lengths in our transistors are macroscopic in dimensions (L = 204 μm); neither an individual P3HT chain

nor a single P3HT crystalline domain is long enough to span the entire channel. Macroscopic charge transport across the channels must thus require interchain transport. Charge transport in the crystalline domain, either along the polymer backbone or in the π-stacking direction, is much faster than charge transport via interchain hopping in the amorphous domain.[33] Despite the presence of amorphous P3HT, the mobility of our P3HT transistors plateaus at a value that is comparable to what had been reported for charge transport within individual crystallites (≈0.01 $cm^2 V^{-1} s^{-1}$).[34–36] We take this observation as indirect evidence to support the assertion that tie chains offer direct intercrystallite transport routes that improve macroscopic charge transport.

In order to elucidate the observed mobility plateau, we investigated the structural order in P3HT thin films through grazing-incidence X-ray diffraction (GIXD). An example of a 2D GIXD pattern of P3HT_5 thin film is shown in **Figure 3a**. Across all P3HT blends, the P3HT crystallites adopt a typical "edge-on" texture in which the alkyl stacking direction is normal to the substrate and π-stacking and the polymer backbone are preferentially oriented in the plane of the substrate,[37] schematically shown in **Figure 3b**. From the GIXD patterns, we quantified the paracrystalline disorder along the π-stacking direction (g_{010}), the dominant interchain transport direction in the crystalline regions. We obtained g_{010} by the single peak-width estimation.[13,38] **Figures 3c-e** show that g_{010} remains largely invariant across the different P3HT blends; a range of 6 to 8% suggests that P3HT exhibits significant paracrystalline disorder along the π-stacking direction in the crystalline domains.[13] For reference, highly-crystalline molecular semiconductors, such as triisopropylsilyl pentacene (TIPS-pentacene), exhibit a paracrystallinity of less than 1%;[38] and glasses, such as SiO_2, exhibit a paracrystallinity of 12%.[39] This comparison suggests that the paracrystalline disorder limits charge transport once sufficient intercrystallite electrical connections have been established for macroscopic charge transport. The effect of local paracrystalline disorder on macroscopic mobility is masked when charge transport is limited by a lack of interdomain connectivity. In a percolated network where the crystallites are sufficiently connected, charge transport is instead limited by the presence of the local structural disorder within crystallites.

In order to further understand the structural disorder exhibited by the P3HT blends, we also performed quantitative analyses of their thin-film absorption spectra according to the Spano model[40,41]. We found that the P3HT aggregates, of which the crystallites are composed, are also similarly disordered along the interchain π-stacking direction (see discussion on the absorption spectra in Supporting Information).

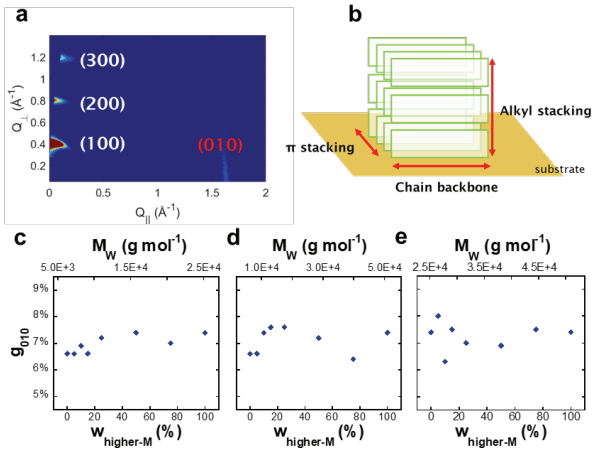

Figure 3. (a) A 2D GIXD pattern of a representative P3HT_5 thin film. The image has been corrected for the "missing wedge" of data along the out-of-plane direction.[42] (b) "Edge-on" texture of P3HT crystallites in which the alkyl stacking direction is normal to the substrate and the π-stacking and polymer backbone are preferentially oriented in the plane of the substrate. Paracrystallinity along the π-stacking direction as a function of the mass fraction of the higher-M P3HT in (c) P3HT_5/20, (d) P3HT_5/40, and (e) P3HT_20/40.

In conclusion, we found a strong correlation between the field-effect mobility of transistors comprising different P3HT blends and their tie-chain fraction, as estimated by the Huang-Brown model. Though the model may be oversimplified for describing the structural origins of mechanical properties of polyolefin blends, we believe the model to be readily applicable for investigating the electrical properties of conjugated polymers. That the field-effect mobility eventually plateaus suggests the presence of sufficient intercrystallite connectivity to establish a percolated network for charge transport, with the plateau mobility limited by the intracrystallite disorder.

Our findings not only demonstrate the intricate balance between interdomain connectivity and intradomain disorder in determining charge-transport properties, but also highlight the critical variables for designing high-mobility polymers. Per the Huang-Brown model, polymers with long (high molar mass) and rigid (long persistence length) chains are more likely to form tie chains. Even without long-range crystalline order, such polymer systems should still afford efficient charge transport,[43] consistent with recent reports that donor-acceptor polymers that are rigid but lack long-range order exhibit high mobilities(over 1 $cm^2 V^{-1} s^{-1}$).[13,44,45] In light of the complex and multifaceted nature of charge transport in conjugated polymers, calculations with the Huang-Brown framework offer a first-order guideline on how to design polymer-chain characteristics and molar mass distributions to optimize charge transport.

ASSOCIATED CONTENT

Supporting Information. This material is available free of charge via the Internet at http://pubs.acs.org: Experimental procedures, the choice of critical length, UV-vis spectroscopy, and transistor measurements and characteristic curves.

AUTHOR INFORMATION

Corresponding Author

* Email: lloo@princeton.edu

Author Contributions

K.G. and Y.-L.L. wrote the manuscript; J.O. and C.K.L. synthesized the P3HT samples; K.G. performed the GIXD measurements, optical absorption measurements, DSC measurements, and fabricated and characterized the field-effect transistors; K.G., C.R.S., A.W.B. and Y.-L.L. conceived the overall scientific framework and discussed the underlying polymer physics; C.R.S. performed the Huang-Brown model calculations. All authors discussed the results and reviewed the manuscript.

Notes

The authors declare no competing financial interest

ACKNOWLEDGMENT

This work was supported by ExxonMobil through its membership in the Princeton E-filliates Partnership of the Andlinger Center for Energy and the Environment. C.K.L. acknowledges NSF DMR 1708317. The P3HT samples were synthesized in part upon work supported by the State of Washington through the University of Washington Clean Energy Institute and via funding from the Washington Research Foundation. A portion of this work was conducted at the Cornell High Energy Synchrotron Source (CHESS), which is supported by the National Science Foundation and the National Institutes of Health/National Institute of General Medical Sciences under NSF award DMR-1332208.

REFERENCES

(1) Flory, P. J.; Yoon, D. Y. Molecular Morphology in Semicrystalline Polymers. *Nature* **1978**, *272*, 226–229.

(2) Lustiger, A.; Markham, R. L. Importance of Tie Molecules in Preventing Polyethylene Fracture under Long-Term Loading Conditions. *Polymer (Guildf).* **1983**, *24*, 1647–1654.

(3) Men, Y.; Rieger, J.; Strobl, G. Role of the Entangled Amorphous Network in Tensile Deformation of Semicrystalline Polymers. *Phys. Rev. Lett.* **2003**, *91*, 1–4.

(4) Guttman, C. M.; DiMarzio, E. A.; Hoffman, J. D. Modelling the Amorphous Phase and the Fold Surface of a Semicrystalline Polymer-the Gambler's Ruin Method. *Polymer (Guildf).* **1981**, *22*, 1466–1479.

(5) Seguela, R. Critical Review of the Molecular Topology of Semicrystalline Polymers: The Origin and Assessment of Intercrystalline Tie Molecules and Chain Entanglements. *J. Polym. Sci. Part B Polym. Phys.* **2005**, *43*, 1729–1748.

(6) Huang, Y.-L.; Brown, N. The Effect of Molecular Weight on Slow Crack Growth in Linear Polyethylene Homopolymers. *J. Mater. Sci.* **1988**, *23*, 3648–3655.

(7) Huang, Y.; Brown, N. Dependence of Slow Crack Growth in Polyethylene on Butyl Branch Density: Morphology and Theory. *J. Polym. Sci. Part B Polym. Phys.* **1991**, *29*, 129–137.

(8) Deslauriers, P. J.; Rohlfing, D. C. Estimating Slow Crack Growth Performance of Polyethylene Resins from Primary Structures Such as Molecular Weight and Short Chain Branching. *Macromol. Symp.* **2009**, *282*, 136–149.

(9) Salleo, A. Charge Transport in Polymeric Transistors. *Mater. Today* **2007**, *10*, 38–45.

(10) Kline, R. J.; McGehee, M. D.; Kadnikova, E. N.; Liu, J.; Fréchet, J. M. J. Controlling the Field-Effect Mobility of Regioregular Polythiophene by Changing the Molecular Weight. *Adv. Mater.* **2003**, *15*, 1519–1522.

(11) Kline, R. J.; McGehee, M. D.; Kadnikova, E. N.; Liu, J.; Fréchet, J. M. J.; Toney, M. F. Dependence of Regioregular Poly(3-Hexylthiophene) Film Morphology and Field-Effect Mobility on Molecular Weight. *Macromolecules* **2005**, *38*, 3312–3319.

(12) Koch, F. P. V.; Rivnay, J.; Foster, S.; Müller, C.; Downing, J. M.; Buchaca-Domingo, E.; Westacott, P.; Yu, L.; Yuan, M.; Baklar, M.; et al. The Impact of Molecular Weight on Microstructure and Charge Transport in Semicrystalline Polymer Semiconductors-Poly(3-Hexylthiophene), a Model Study. *Prog. Polym. Sci.* **2013**, *38*, 1978–1989.

(13) Noriega, R.; Rivnay, J.; Vandewal, K.; Koch, F. P. V; Stingelin, N.; Smith, P.; Toney, M. F.; Salleo, A. A General Relationship between Disorder, Aggregation and Charge Transport in Conjugated Polymers. *Nat. Mater.* **2013**, *12*, 1038–1044.

(14) Himmelberger, S.; Vandewal, K.; Fei, Z.; Heeney, M.; Salleo, A. Role of Molecular Weight Distribution on Charge Transport in Semiconducting Polymers. *Macromolecules* **2014**, *47*, 7151–7157.

(15) Bronstein, H. A.; Luscombe, C. K. Externally Initiated Regioregular P3HT with Controlled Molecular Weight and Narrow Polydispersity. *J. Am. Chem. Soc.* **2009**, *131*, 12894–12895.

(16) Gu, K.; Onorato, J.; Xiao, S. S.; Luscombe, C. K.; Loo, Y.-L. Determination of the Molecular Weight of Conjugated Polymers with Diffusion-Ordered NMR Spectroscopy. *Chem. Mater.* **2018**, *30*, 570–576.

(17) Joseph Kline, R.; McGehee, M. D.; Toney, M. F. Highly Oriented Crystals at the Buried Interface in Polythiophene Thin-Film Transistors. *Nat. Mater.* **2006**, *5*, 222–228.

(18) Vakhshouri, K.; Smith, B. H.; Chan, E. P.; Wang, C.; Salleo, A.; Wang, C.; Hexemer, A.; Gomez, E. D. Signatures of Intracrystallite and Intercrystallite Limitations of Charge Transport in Polythiophenes. *Macromolecules* **2016**, *49*, 7359–7369.

(19) Chew, A. R.; Ghosh, R.; Pakhnyuk, V.; Onorato, J.; Davidson, E. C.; Segalman, R. A.; Luscombe, C. K.; Spano, F. C.; Salleo, A. Unraveling the Effect of Conformational and Electronic Disorder in the Charge Transport Processes of Semiconducting Polymers. *Adv. Funct. Mater.* **2018**, *28*, 1804142.

(20) Fischer, E. W. Studies of Structure and Dynamics of Solid Polymers by Elastic and Inelastic Neutron Scattering. *Pure Appl. Chem.* **1978**, *50*, 1319–1341.

(21) Vakhshouri, K.; Gomez, E. D. Effect of Crystallization Kinetics on Microstructure and Charge Transport of Polythiophenes. *Macromol. Rapid Commun.* **2012**, *33*, 2133–2137.

(22) Duong, D. T.; Ho, V.; Shang, Z.; Mollinger, S.; Mannsfeld, S. C. B.; Dacuna, J.; Toney, M. F.; Segalman, R.; Salleo, A. Mechanism of Crystallization and Implications for Charge Transport in Poly(3-Ethylhexylthiophene) Thin Films. *Adv. Funct. Mater.* **2014**, *24*, 4515–4521.

(23) Mcculloch, B.; Ho, V.; Hoarfrost, M.; Stanley, C.; Do, C.; Heller, W. T.; Segalman, R. A. Polymer Chain Shape of Poly(3-Alkylthiophenes) in Solution Using Small-Angle Neutron Scattering. *Macromolecules* **2013**, *46*, 1899–1907.

(24) Rubinstein, M.; Colby, R. H. *Polymer Physics*, 1st ed.; Oxford University Press: New York, 2003.

(25) Broadhurst, M. G. Extrapolation of the Orthorhombic N-Paraffin Melting Properties to Very Long Chain Lengths. *J. Chem. Phys.* **1962**, *36*, 2578–2582.

(26) Snyder, C. R.; Nieuwendaal, R. C.; DeLongchamp, D. M.; Luscombe, C. K.; Sista, P.; Boyd, S. D. Quantifying Crystallinity in High Molar Mass Poly(3-Hexylthiophene). *Macromolecules* **2014**, *47*, 3942–3950.

(27) Brinkmann, M.; Wittmann, J.-C. Orientation of Regioregular Poly(3-Hexylthiophene) by Directional Solidification: A Simple Method to Reveal the Semicrystalline Structure of a Conjugated Polymer. *Adv. Mater.* **2006**, *18*, 860–863.

(28) Crist, B.; Mirabella, F. M. Crystal Thickness Distributions from Melting Homopolymers or Random Copolymers. *J. Polym. Sci. Part B Polym. Phys.* **1999**, *37*, 3131–3140.

(29) Lee, C. S.; Dadmun, M. D. Important Thermodynamic Characteristics of Poly(3-Hexyl Thiophene). *Polymer (Guildf).* **2014**, *55*, 4–7.

(30) Huang, Y.; Brown, N. The Dependence of Butyl Branch Density on Slow Crack Growth in Polyethylene: Kinetics. *J. Polym. Sci. Part B Polym. Phys.* **1990**, *28*, 2007–2021.

(31) Yeh, J. T.; Runt, J. Fatigue Crack Propagation in High-Density Polyethylene. *J. Polym. Sci. Part B Polym. Phys.* **1991**, *29*, 371–

388.
(32) Patel, R. M.; Sehanobish, K.; Jain, P.; Chum, S. P.; Knight, G. W. Theoretical Prediction of Tie-Chain Concentration and Its Characterization Using Postyield Response. *J. Appl. Polym. Sci.* **1996**, *60*, 749–758.
(33) Mollinger, S. A.; Krajina, B. A.; Noriega, R.; Salleo, A.; Spakowitz, A. J. Percolation, Tie-Molecules, and the Microstructural Determinants of Charge Transport in Semicrystalline Conjugated Polymers. *ACS Macro Lett.* **2015**, *4*, 708–712.
(34) Merlo, J. a.; Frisbie, C. D. Field Effect Conductance of Conducting Polymer Nanofibers. *J. Polym. Sci. Part B - Polym. Phys.* **2003**, *41*, 2674.
(35) Merlo, J. A.; Frisbie, C. D. Field Effect Transport and Trapping in Regioregular Polythiophene Nanofibers. *J. Phys. Chem. B* **2004**, *108*, 19169–19179.
(36) Kim, D. H.; Jang, Y.; Park, Y. D.; Cho, K. Controlled One-Dimensional Nanostructures in Poly(3-Hexylthiophene) Thin Film for High-Performance Organic Field-Effect Transistors. *J. Phys. Chem. B* **2006**, *110*, 15763–15768.
(37) Sirringhaus, H.; Brown, P. J.; Friend, R. H.; Nielsen, M. M.; Bechgaard, K.; Langeveld-Voss, B. M. W.; Spiering, a. J. H.; Janssen, R. a. J.; Meijer, E. W.; Herwig, P.; et al. Two-Dimensional Charge Transport in Self-Organized, High-Mobility Conjugated Polymers. *Nature* **1999**, *401*, 685–688.
(38) Rivnay, J.; Noriega, R.; Kline, R. J.; Salleo, A.; Toney, M. F. Quantitative Analysis of Lattice Disorder and Crystallite Size in Organic Semiconductor Thin Films. *Phys. Rev. B - Condens. Matter Mater. Phys.* **2011**, *84*, 1–20.
(39) Hindeleh, A. M.; Hosemann, R. Microparacrystals: The Intermediate Stage between Crystalline and Amorphous. *J. Mater. Sci.* **1991**, *26*, 5127–5133.
(40) Spano, F. C. Modeling Disorder in Polymer Aggregates: The Optical Spectroscopy of Regioregular Poly(3-Hexylthiophene) Thin Films. *J. Chem. Phys.* **2005**, *122*, 234701.
(41) Spano, F. C. Absorption in Regio-Regular Poly(3-Hexyl)Thiophene Thin Films: Fermi Resonances, Interband Coupling and Disorder. *Chem. Phys.* **2006**, *325*, 22–35.
(42) Baker, J. L.; Jimison, L. H.; Mannsfeld, S.; Volkman, S.; Yin, S.; Subramanian, V.; Salleo, A.; Alivisatos, A. P.; Toney, M. F. Quantification of Thin Film Crystallographic Orientation Using X-Ray Diffraction with an Area Detector. *Langmuir* **2010**, *26*, 9146–9151.
(43) Snyder, C. R.; DeLongchamp, D. M. Glassy Phases in Organic Semiconductors. *Curr. Opin. Solid State Mater. Sci.* **2018**, *22*, 41–48.
(44) Tsao, H. N.; Cho, D.; Andreasen, J. W.; Rouhanipour, A.; Breiby, D. W.; Pisula, W.; Müllen, K. The Influence of Morphology on High-Performance Polymer Field-Effect Transistors. *Adv. Mater.* **2009**, *21*, 209–212.
(45) Zhang, X.; Bronstein, H.; Kronemeijer, A. J.; Smith, J.; Kim, Y.; Kline, R. J.; Richter, L. J.; Anthopoulos, T. D.; Sirringhaus, H.; Song, K.; et al. Molecular Origin of High Field-Effect Mobility in an Indacenodithiophene-Benzothiadiazole Copolymer. *Nat. Commun.* **2013**, *4*, 2238.

Insert Table of Contents artwork here

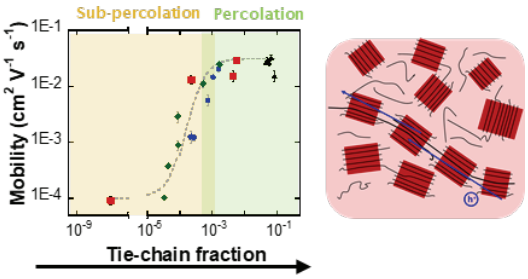

Supporting Information

Assessing the Huang-Brown Description of Tie Chains for Charge Transport in Conjugated Polymers

Kaichen Gu[†], Chad R. Snyder[‖], Jonathan Onorato[‡], Christine K. Luscombe[‡,#,^], August W. Bosse[§], Yueh-Lin Loo[†,⊥,*]

[†] Department of Chemical and Biological Engineering, Princeton University, Princeton, New Jersey 08544, United States

[‖] Materials Science and Engineering Division, National Institute of Standards and Technology, Gaithersburg, Maryland 20899, United States

[‡] Materials Science and Engineering Department, University of Washington, Seattle, Washington 98195-2120, United States

[§] Corporate Strategic Research, ExxonMobil Research and Engineering Company, Annandale, New Jersey 08801, United States

[#]Department of Chemistry, University of Washington, Seattle, Washington 98195-1700, United States

[^]Molecular Engineering and Sciences Institute, University of Washington, Seattle, Washington 98195-1652, United States

⊥ Andlinger Center for Energy and the Environment, Princeton University, Princeton, New Jersey 08544, United States

* Email: lloo@princeton.edu

Content

I. Experimental procedures

Materials: All solvents were purchased from Fisher Scientific and used as-received.[1] Hexamethyldisilazane (HMDS) was purchased from Sigma Aldrich and used as-received. P3HT was synthesized per literature, resulting in tolyl-group initiated 100% regioregular P3HT.[2,3] The molar masses and molar-mass distributions of the four regioregular P3HT samples (P3HT_5, P3HT_10, P3HT_20, and P3HT_40) were characterized by SEC and NMR end-group analysis separately and their absolute molar masses and dispersities are provided in **Table S1**.

Table S1. Summary of the molar masses of P3HT obtained by size exclusion chromatography and NMR end-group analysis.

Samples	M_n [kg mol^{-1}][a)]	$Đ$ [-][b)]	M_w [kg mol^{-1}][c)]
P3HT_5	5.0	1.26	6.3
P3HT_10	10.0	1.17	11.7
P3HT_20	20.0	1.26	25.2
P3HT_40	40.0	1.27	51.0

[a)] The number average molar mass (M_n) is determined by NMR end-group analysis; [b)] the dispersity ($Đ$) is determined by size exclusion chromatograph; [c)] the mass average molar mass (M_w) is calculated by multiplying the M_n by $Đ$.

Differential Scanning Calorimetry: DSC scans were collected using a TA Instruments Q2000 DSC with Tzero aluminum sample and reference pans. P3HT was fully dissolved in chloroform and high- and low- M solutions were fully mixed in controlled mass ratios before directly drop-casted into the DSC pans. We scanned between (25 and 270) °C at a rate of 10 °C min^{-1} for two heating and cooling cycles.

Transistor Fabrication and Characterization: All thin-film transistors were fabricated in a bottom-gate-top-contact manner. Si (100) wafers with 300 nm thermally-grown SiO_2 (purchased from Process Specialties, Inc.) were used as gate and gate dielectric, respectively. The substrates were cleaned by sonication in deionized water, acetone, isopropanol for 5 minutes each and then dried with nitrogen stream. Their oxide surfaces were modified by spin-coating HMDS at 60π rad/s

(1800 rpm), followed by thermal annealing at 120 °C for 5 min. P3HT was drop-casted (0.5 mg mL^{-1} solution in chloroform) onto the substrates at ambient conditions. 50 nm of gold was then thermally evaporated onto the substrates at a rate of ≈1.5 A s^{-1}, through a stencil mask to define active channels with a width of 204 μm and a channel length of 50 μm. All transistors were tested under vacuum using an Agilent 4155C semiconductor parameter analyzer. The hole mobilities were estimated in the saturation regime at a source-drain voltage of -80 V.

Grazing-Incidence X-Ray Diffraction: P3HT thin films for GIXD were deposited in the same manner as described above. GIXD was performed at the G2 station at the Cornell High Energy Synchrotron Source. X-rays at 13.0 keV were selected using a beryllium single-crystal monochromator. A 0.2 × 3 (V × H) mm^2 beam was defined with motorized slits. The X-ray beam was aligned between the critical angles of the film and substrate, at 0.175° with respect to the substrate. Scattered intensity was collected using a 640-element 1D diode array. All GIXD images have been background subtracted.

Optical Absorption Measurements: P3HT thin films were drop-casted onto glass slides in the same manner as described above. Absorption spectra were recorded using an Agilent Technologies Cary 5000 spectrophotometer.

II. The choice of critical length

In applying the statistical approach outlined in our manuscript, we needed to define the critical distance beyond which a tie chain can be established, corresponding to the minimum distance that tie chains need to span in order to electrically bridge two neighboring crystalline domains. In previous studies, both $(2l_c+l_a)$[4,5] and $(2l_c+2l_a)$[6] were used as critical distances in assessing the tie-chain fraction of polyethylene resins. Polyethylene adopts an alternating crystalline-amorphous lamellar structure with an amorphous layer thickness, l_a, corresponding to the edge-to-edge distance between two neighboring crystalline domains; this distance specifies the lower bound for the distance across which tie chains need to form.[4] Because 90% of chain ends are excluded from polyethylene crystallites, a more reasonable critical distance is given by $(2l_c+l_a)$.[7] While it is unclear whether the chain ends reside in the crystalline domains or the amorphous regions in P3HT, we hypothesize that it is easier for P3HT to accommodate its chain ends in its crystalline domains compared to polyethylene in our case because of the tolyl end groups in our 100% regioregular P3HT are comparable in size with thiophene mers. We thus surmise the critical distance for tie-chain formation in P3HT to be between l_a and $(2l_c+l_a)$.

In order to assess how the choice of critical distance impacts the calculated tie chain fraction, we performed a sensitivity analysis on our calculation of the tie-chain fraction in P3HT_5/40. **Figure S1a** shows the distribution of f_{TC} when the critical distance is varied. In this particular case, we varied the l_c contribution. We see that the absolute value of the calculated tie-chain fraction strongly depends on the choice of critical distance, with larger critical distances resulting in smaller f_{TC}. f_{TC} increases by more than an order of magnitude when the critical distance is reduced from $(2l_c+l_a)$ to $(0.5l_c+l_a)$. However, variations in l_c have much less of an effect on the relative f_{TC}.[8] We also investigated the distribution of f_{TC} by varying l_a, as shown in **Figure S1b**.

In a similar vein, we found the relative tie-chain fraction to be insensitive to variations in l_a. Our sensitivity analysis of the different possible critical distance

scenarios implies a robustness of the model on the relative tie-chain fraction, although different end-group chemistries can ultimately dictate chain-end location and impact the critical distance over which tie chains form.

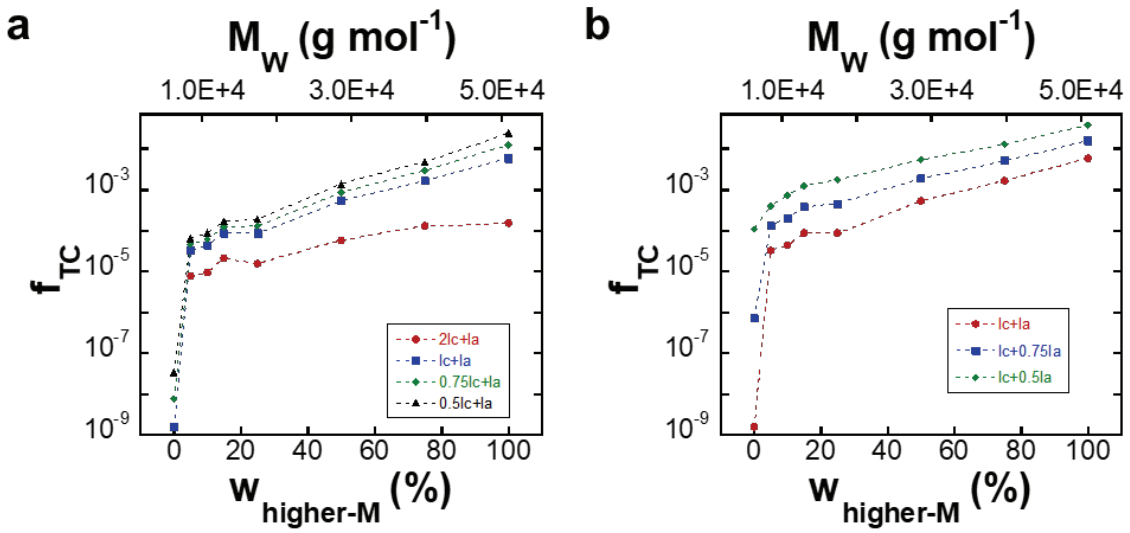

Figure S1. The distribution in tie-chain fraction (f_{TC}) of P3HT_5/40 when different critical distances, by varying (a) the crystalline domain thickness and (b) the characteristic distance between crystalline domains, are used during analysis.

As outlined in the main text, the Huang-Brown model assumes that a polymer chain forms a tie chain when its end-to-end distance is greater than, or equal to, the critical distance (d_c). As opposed to the end-to-end distance, the probability function in Equation (1) is formulated using the diameter of gyration (d_g) as the polymer characteristic size.[9] For linear polymers, the end-to-end distance is related to diameter of gyration by:

$$R = \frac{\sqrt{6}}{2} d_g \cong 1.22\, d_g \qquad (S1)$$

Hence, if the criterion for forming a tie chain were that the diameter of gyration is greater than, or equal to, the critical distance ($d_g \geq d_c$), the probability of forming a tie chain described by Equation (1) can be modified accordingly:

$$P(M) = \frac{\int_{1.22d_c}^{\infty} r^2 \exp\left(-\frac{3r^2}{2Nl_K^2}\right) dr}{\int_0^{\infty} r^2 \exp\left(-\frac{3r^2}{2Nl_K^2}\right) dr} \qquad (S2)$$

The model is probabilistically equivalent under the following two scenarios: (a) using the polymer diameter of gyration as the polymer characteristic size and a critical distance of d_c, and (b) using the polymer end-to-end distance as the polymer characteristic size and a critical distance of $1.22d_c$. The impact of using either of these polymer characteristic sizes is assessed through sensitivity tests performed on the choice of critical lengths.

III. UV-vis spectroscopy

Detailed quantitative analysis of the absorption spectra of P3HT blends can provide further insight into the thin-film structure.[10,11] The absorption spectra of drop-cast P3HT thin films were fitted with a weakly coupled H-aggregate model developed by Spano and co-workers to extract the Gaussian line width (σ) and the free exciton bandwidth (W). [10–13] The fittings of the spectra of P3HT_5/20 blends per the Spano model are shown in **Figure S2**. σ measures the extent of interchain disorder within P3HT aggregates; **Figures S3a-c** show that this quantity does not vary significantly or systematically across the different blends, suggesting that the P3HT aggregates are similarly disordered along the interchain π-stacking direction. The free exciton bandwidth, W, varies inversely with the number of interacting thiophene units in these aggregates along the backbone direction and hence gives a measure of the conjugation length and intrachain order.[14] W in both P3HT_5/20 (**Figure S3d**) and P3HT_5/40 (**Figure S3e**) gradually decreases with increasing loadings of higher-M fraction, suggesting better intrachain order within the aggregates as the loading of the higher-M fraction increases, consistent with previous reports.[15] Decreasing exciton bandwidth contributes to enhanced charge transport and the change in W is only moderate upon the initial loading of higher-M fraction (up to 25%), compared to the initial sharp increase in mobility. We argue that the lack of interdomain connectivity is still the bottleneck for charge transport in these samples. The molecular-weight dependence of W for P3HT_20/40 is less pronounced: W stays at values much lower than that of P3HT_5 (**Figure S3f**), suggesting a similar extent of order along the polymer backbone in drop-cast films of P3HT with M_n > 20 kg mol^{-1}.

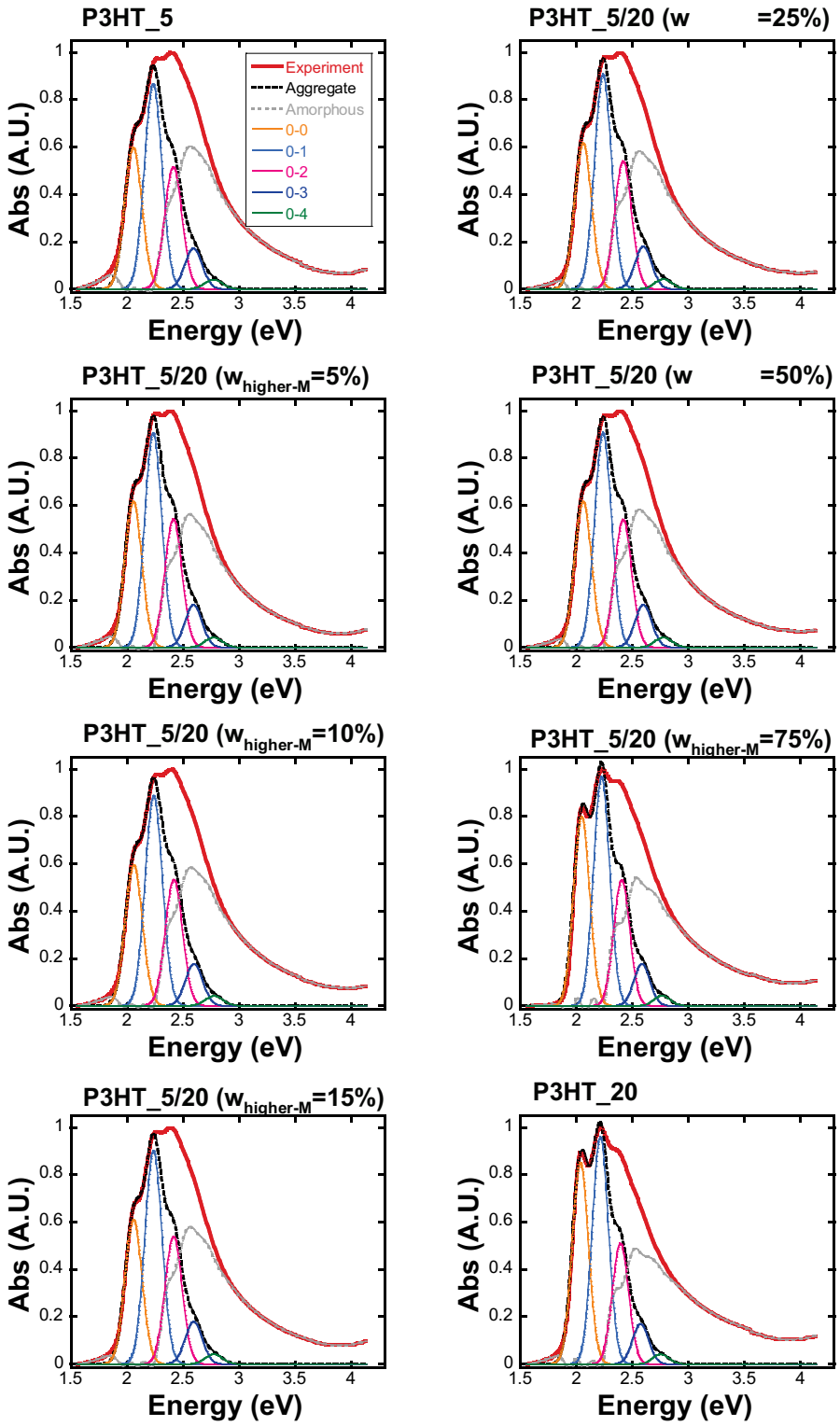

Figure S2. The experimental UV-vis absorption spectra of P3HT_5/20. The aggregate and amorphous components are deconvoluted per the Spano model.

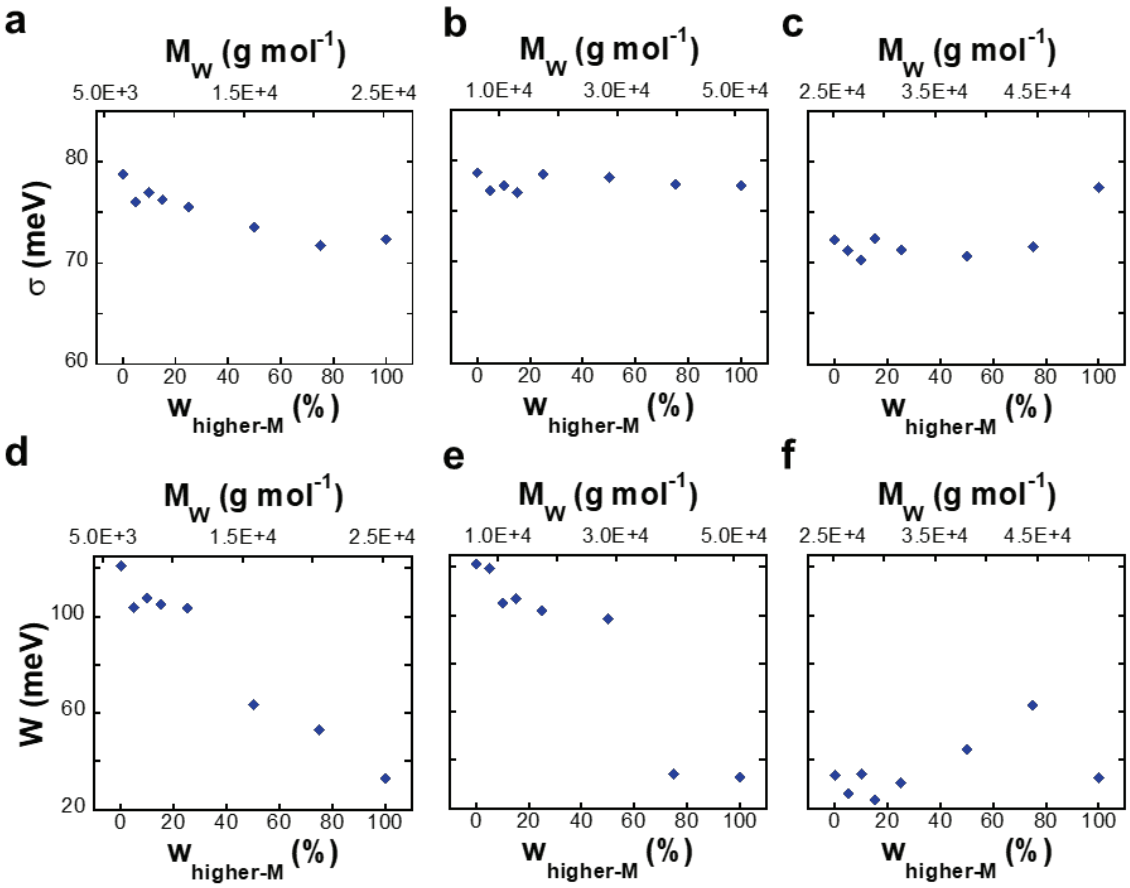

Figure S3. Gaussian line width as a function of the fraction of the higher-MW P3HT in (a) P3HT_5/20, (b) P3HT_5/40, and (c) P3HT_20/40. Free exciton bandwidth as a function of the fraction of the higher-MW P3HT in (d) P3HT_5/20, (e) P3HT_5/40, and (f) P3HT_20/40. Both the Gaussian line width and the free exciton bandwidth were extracted from their respective absorbance data per the Spano model.

IV. Transistor measurements and characteristic curves

The field-effect mobility is the main figure of merit of an organic field-effect transistor;[16] it describes how quickly charges move through the semiconducting active layer under an applied electric field. The mobilities in this study are calculated from the transfer characteristics in the saturation regime, according to the following equation:[17]

$$I_D = \frac{C_i W}{2L} \mu (V_G - V_T)^2 \qquad (S3)$$

where I_D is the source-drain current; C_i is the capacitance of the dielectric layer (11.7 nF cm^{-2} for 300-nm thermally-grown silicon oxide); W and L are the channel width and length, respectively; V_G is the gate voltage; and V_T is the threshold voltage. The mobility is extracted from the slope of $|I_D|^{1/2}$ versus V_G once the device is turned on. Representative transfer and output curves are shown in **Figure S4**.

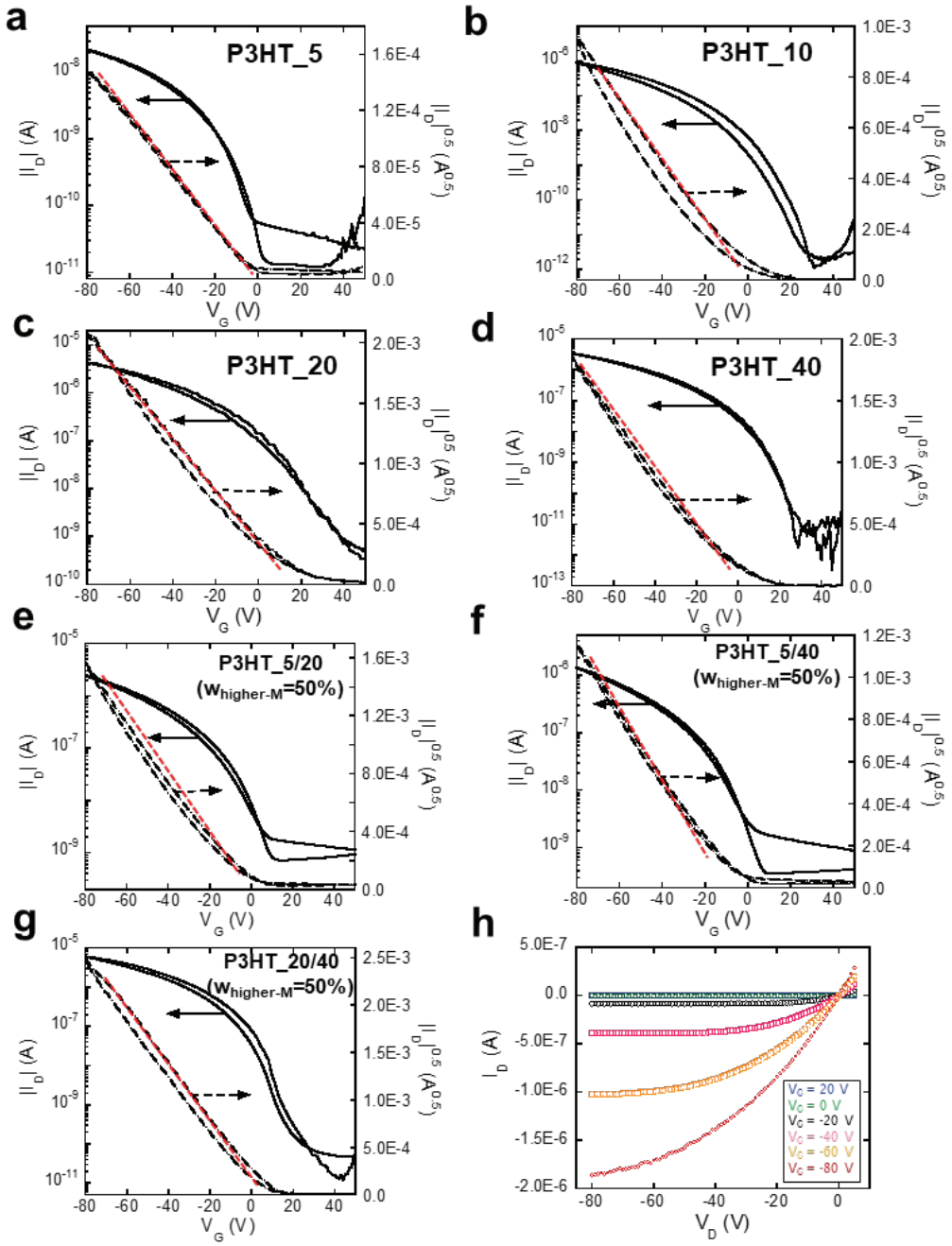

Figure S4. (a-g) Representative transfer curves of transistors comprising P3HT_5, P3HT_10, P3HT_20, P3HT_40, P3HT_5/20 ($w_{higher\text{-}M}$=50%), P3HT_5/40 ($w_{higher\text{-}M}$=50%), P3HT_20/40 ($w_{higher\text{-}M}$=50%) respectively. The devices were measured in the saturation regime at a source-drain voltage of -80 V. The mobility values were calculated from the slope of $|I_D|^{1/2}$ versus V_G (red dashed lines). (h) Representative output curve of transistors comprising P3HT_40, taken at varying source-gate voltages.

V. References

1. Certain commercial equipment, instruments, or materials are identified in this paper in order to specify the experimental procedure adequately. Such identification is not intended to imply recommendation or endorsement by the National Institute of Standards and Technology, nor is it intended to imply that the materials or equipment identified are necessarily the best available for the purpose.
2. Bronstein, H. A. & Luscombe, C. K. Externally Initiated Regioregular P3HT with Controlled Molecular Weight and Narrow Polydispersity. *J. Am. Chem. Soc.* **131,** 12894–12895 (2009).
3. Gu, K., Onorato, J., Xiao, S. S., Luscombe, C. K. & Loo, Y.-L. Determination of the Molecular Weight of Conjugated Polymers with Diffusion-Ordered NMR Spectroscopy. *Chem. Mater.* **30,** 570–576 (2018).
4. Huang, Y. & Brown, N. The dependence of butyl branch density on slow crack growth in polyethylene: Kinetics. *J. Polym. Sci. Part B Polym. Phys.* **28,** 2007–2021 (1990).
5. Deslauriers, P. J. & Rohlfing, D. C. Estimating slow crack growth performance of polyethylene resins from primary structures such as molecular weight and short chain branching. *Macromol. Symp.* **282,** 136–149 (2009).
6. Huang, Y.-L. & Brown, N. The effect of molecular weight on slow crack growth in linear polyethylene homopolymers. *J. Mater. Sci.* **23,** 3648–3655 (1988).
7. Keller, A. & Priest, D. J. Experiments on the Location of Chain Ends in Monolayer Single Crystals of Polyethylene. *J. Macromol. Sci. Part B* **2,** 479–495 (1968).
8. Huang, Y. & Brown, N. Dependence of slow crack growth in polyethylene on butyl branch density: Morphology and theory. *J. Polym. Sci. Part B Polym. Phys.* **29,** 129–137 (1991).
9. Yeh, J. T. & Runt, J. Fatigue crack propagation in high-density polyethylene. *J. Polym. Sci. Part B Polym. Phys.* **29,** 371–388 (1991).
10. Spano, F. C. Modeling disorder in polymer aggregates: The optical spectroscopy of regioregular poly(3-hexylthiophene) thin films. *J. Chem. Phys.* **122,** 234701 (2005).

11. Spano, F. C. Absorption in regio-regular poly(3-hexyl)thiophene thin films: Fermi resonances, interband coupling and disorder. *Chem. Phys.* **325,** 22–35 (2006).
12. Clark, J., Chang, J. F., Spano, F. C., Friend, R. H. & Silva, C. Determining exciton bandwidth and film microstructure in polythiophene films using linear absorption spectroscopy. *Appl. Phys. Lett.* **94,** 2007–2010 (2009).
13. Turner, S. T. *et al.* Quantitative analysis of bulk heterojunction films using linear absorption spectroscopy and solar cell performance. *Adv. Funct. Mater.* **21,** 4640–4652 (2011).
14. Gierschner, J. *et al.* Excitonic versus electronic couplings in molecular assemblies : The importance of non-nearest neighbor interactions. *J. Chem. Phys.* **130,** 044105 (2009).
15. Pingel, P. *et al.* Temperature-resolved local and macroscopic charge carrier transport in thin P3HT layers. *Adv. Funct. Mater.* **20,** 2286–2295 (2010).
16. Sirringhaus, H. 25th Anniversary Article: Organic field-effect transistors: The path beyond amorphous silicon. *Adv. Mater.* **26,** 1319–1335 (2014).
17. Horowitz, G. Organic field-effect transistors. *Adv. Mater.* **10,** 365–377 (1998).